



Cold spray surface patterning of aluminum on aluminum, silicon, glass, and printed circuit board substrates

Chun-Hsien Wu*, Jonathan E. Palao

Naval Postgraduate School, Mechanical and Aerospace Engineering, Monterey, CA 93943, United States of America



ARTICLE INFO

Keywords:
Cold spray
Surface patterning
Surface modification
Functional coating
Monte Carlo simulation

ABSTRACT

The aim of the present study is to investigate the feasibility and the criteria of using the cold spray technique for surface patterning to create two-dimensional surface features on various substrates. Metal meshes (16, 45, 170, 200, 400, and 5/16") were used as screens for surface patterning in this investigation; fabricated features were characterized with optical microscope, scanning electron microscope, and optical profilometer. Processing parameters like mesh size, standoff distance, gun traverse speed, and number of spray passes were examined to study their influence to the morphology of the fabricated features. Two-dimensional aluminum features were successfully fabricated on aluminum, soda-lime glass, silicon wafer, and the copper foil-layer of printed circuit board. The smallest feature created with –45 to +5 µm aluminum feedstock powders, has an average size of 67.4 µm. It was determined that the pore size of a mesh needs to be at least 3.3 times bigger than the average size of feedstock powders in order to create features successfully. To estimate the probability of feedstock powders passing through a mesh and simulate the topography of the fabricated features, a Monte Carlo simulation incorporating the particle size distribution and the geometries of meshes was developed. With the capability of creating features on diverse substrates, the cold spray surface patterning technique shows promising potential to create heterogeneous two-dimensional functional features or devices at micron-sized with high efficiency.

1. Introduction

Cold gas dynamic spray is a solid state coating technique. The feedstock powders are injected into a convergent-divergent (de Laval) nozzle and accelerated by high pressure gas (most commonly compressed air, nitrogen, or helium) to supersonic speed (200 to 1200 m/s) [1–3]. Once the impact velocities of the feedstock powders exceed critical velocity [1] [4, 5], the powders adhere to the substrate with plastic deformation, instead of bouncing back. Assadi et al. suggested that thermal softening and adiabatic shear instability at the interface of particle and substrate play an important role in the bonding formation of cold spray [4] [6, 7]. Cold spray is conducted at relatively low temperatures compared to thermal spray. No melting of feedstock powders is involved in the deposition process, and the particle impact temperature is relatively low. A dense coating with low oxide content can be formed with this technique. Besides the benefits of a low processing temperature, coatings of various materials such as metals, metal matrix composites, ceramics, polymers, and nanomaterials, can be fabricated with cold-gas dynamic spray on various substrates, including metals, ceramics, semiconductors, and polymers [8–10].

Cold spray is a surface-coating technique, which is commonly used

to produce: wear resistant, corrosion resistant, thermal barrier, anti-fouling, and conductive/nonconductive (electrical and thermal) coatings [8–15]. In addition to forming functional coatings, cold spray is also well-known for its capability to restore damaged parts to their original dimensions, also known as additive repairing [16]. With this capability, the part can be restored to a functional condition instead of replacing an expensive damaged part entirely. In practice, a corroded gear box of a Seahawk helicopter was restored by cold spray, which provided a cost savings of 35–50% [17]. Along to its repairing capabilities, cold spray is also known for its potential in additive manufacturing [18]. Recently M. E. Lynch et al. have demonstrated a designing and optimizing process for cold spray additive manufacturing for a part with 20% reduction in weight [19]. All previously described applications of cold spray focused on the fabrication of functional coatings, additive repairing, and additive manufacturing; however, the potential of using cold spray as a surface patterning technique was rarely explored.

Some of widely known surface patterning techniques for preparing and creating patterns on surfaces from the arrangement of single atom to the macro-scale features include etching, laser patterning, film deposition, and lithography [20–27]. Etching, laser patterning, and

* Corresponding author at: 700 Dyer Road, Watkins Hall, Building 245, Room 239, Naval Postgraduate School, Monterey, CA 93943, United States of America.
E-mail address: will172@vt.edu (C.-H. Wu).

lithography mostly pattern surfaces by removal of materials [21–27]. The film deposition techniques such as physical vapor deposition and chemical vapor deposition require systems under vacuum; the surface area that can be patterned is typically limited by the space in a system chamber [22] [28, 29]. Cold spray does not require vacuum and has high deposition efficiency. A coating of hundreds of microns can be deposited on a square inch area within a few seconds. Moreover, the system can be designed to be portable and be used in field. By incorporating a screen in cold spray process, cold spray can be used to create bottom-up surface patterns. Several studies have been reported regarding the surface patterning using cold spray; D. Kim et al. have used cold spray to deposit one-dimensional copper lines with widths varying from 150 to 1500 μm on silicon wafer and soda-lime glass to explore the potential of cold spray technology to print electrodes in solar cell applications [10]; S. V. Klinkov et al. studied cold spray through a mask (wire) with transverse size in the range 0.3–1 mm to produce one-dimensional non-conductive path (region with no coating) [30]; Y. Cormier et al. explored the manufacturability of two dimensional fin arrays from 12 to 30 fins/in to serve as compact heat exchanger by cold spray process using steel wire mesh [31–33]. The prior publications focused on production of one-dimensional features and the heat exchanger application of cold sprayed fins. The current study focuses on the fabrication of two-dimensional surface patterns through metal screens (metal meshes) to explore the influence of particle size of feedstock powders, pore and wire size of meshes, standoff distance, gun temperature, gun pressure, and gun traverse speed to the geometries of the patterned features on various substrates. The aim of the present study includes investigation of how small a two-dimensional surface feature can be fabricated with metal meshes and commercial aluminum powders, the ratio of the pore size of a mesh to the average particle size of feedstock powders for successful cold spray deposition, how geometries of the features can be modified, and what substrate (aluminum, glass, silicon wafer, and printed circuit board) can be patterned using cold spray surface patterning technique. The cold sprayed features were characterized by optical microscopy, scanning electron microscopy (SEM), and optical profilometer. A Monte Carlo simulation was developed to evaluate the deposition probability of feedstock powders

passing through the meshes and simulate the morphologies of patterned features.

2. Material and methods

The cold spray patterning experiments were carried out on a Centerline SST series C low pressure cold spray system (< 300 psi) with cabinet and robotic control [34]. UltiFlow polymer nozzle with length of 120 mm, orifice size of 2 mm), and maximum operation temperature of 350 °C was used to spray feedstock powders in all the cold spray experiments. The feedstock powders used in the experiments are aluminum 3 μm from Pyro Chem Source, 5 μm from Alpha Chemicals, and –45 to +5 μm (Al 99.5 Min., SST - A5001) from Centerline. The screens used are 200 (75 μm) and 400 (37 μm) 316 stainless steel meshes from Beyondsupply; 5/16" (8 mm.) mesh from Surplus EQ Co., 16 (1190 μm) and 170 (88 μm) copper meshes from Deal MFG. Co., 45 (355 μm) mesh from Advantech Co, and 3D printed 8 mm ABS (Acrylonitrile Butadiene Styrene) mesh. The carrier gas used in this investigation was high purity nitrogen. The nozzle inlet pressure was 1.38 MPa and nozzle inlet temperatures ranged between 150 and 300 °C. The substrates tested were 1100 series aluminum, silicon wafer from Montco Silicon Tech, soda-lime glass from Ted Pella Inc., and printed circuit board from Uxcell. All substrates were cleaned with acetone before use, and no surface treatment such as grit blasting was applied to the substrates. All the processing parameters for cold spray surface patterning experiments on these substrates are listed in Table 1, Table 2, and Table 3.

The morphology of the patterned substrates was analyzed with a Dino-Lite digital microscope for low magnification imaging. Nikon Epiphot 200 metallographic optical microscope and the Zeiss Neon 40 field emission scanning electron microscope were used to measure the feature size of the fabricated features and the pore size of the meshes at high magnification. The particles size of the feedstock powders was analyzed by laser scattering particle size distribution analyzer: LA-950V2, HORIBA. The feature heights and three-dimensional topography of the features were characterized by Zygo NewView 7100 optical profilometer. All the measurements were conducted in Image J

Table 1

Cold spray processing parameters and feature height of features fabricated with meshes, 16, 170, 200, and 400, on aluminum substrate.

Sample ID	Al-1	Al-2	Al-3	Al-4	Al-5	Al-6	Al-7	Al-8
Mesh	16	16 ^a	16	170	170	200	200	400
Pressure (Psi)	200	200 ^a	200	160	200	200	200	200
Gas temp. (°C)	320	320 ^a	320	150	300	300	300	300
Feed rate (%)	40	40 ^a	40	15	20	15	20	20
Gun traverse speed (mm/s)	10	10 ^a	20	20	20	20	40	20
Standoff distance nozzle – mesh (mm.)	25	25 ^a	25	15	25	25	25	15
Standoff Distance mesh –Substrate (mm.)	2	2 ^a	2	0	0	0	0	0
Feature height (μm)	392.3 ± 9.5	760.6 ± 25.6 ^a	59.9 ± 2.1	N/A ^b	12.0 ± 0.8	8.8 ± 1.2	11.5 ± 2.2	N/A ^b

^a The only data set fabricated with two passes.

^b No adhesion of powders.

Table 2

Cold spray processing parameters and feature height of features fabricated with meshes, 5/16", 16, and 45, on glass and silicon wafer substrates.

Sample ID	Glass-1	Si-2	Si-3	Si-4	Si-5	Si-6
Mesh	16 ^a	5/16"	16	16	45	45
Pressure (Psi)	200 ^a	200	200	200	200	200
Gas temp. (°C)	320 ^a	320	245	245	245	245
Feed rate (%)	40 ^a	20	20	20	20	20
Gun traverse speed (mm/s)	20 ^a	40	40	40	40	40
Standoff distance nozzle – mesh (mm.)	50 ^a	50	25	25	25	25
Standoff distance mesh –substrate (mm.)	3.58 ^a	11	1	2.37	0	2.37
Feature height (μm)	589.1 ± 165.5 ^a	58.57 ± 9.1	157.8 ± 2.1	175.2 ± 5.5	33.4 ± 3.0	156.9 ± 4.7

^a The only data set fabricated on glass substrate.

Table 3

Cold spray processing parameters and feature height of features fabricated with meshes, 16 and 45, on copper foil layer of PCB.

Sample ID	PCB-1	PCB-2	PCB-3	PCB-4	PCB-5	PCB-6	PCB-7
Mesh	16	45	45	45	45	45	45
Pressure (Psi)	200	200	200	200	200	200	200
Gas temp. (°C)	245	245	245	245	245	245	245
Feed rate (%)	20	10	20	20	20	20	10
Gun traverse speed (mm/s)	20	20	20	20	40	40	20
Standoff distance nozzle – mesh (mm.)	25	25	25	25	25	25	25
Standoff distance mesh –Substrate (mm.)	1.7	1.7	1.7	3.7	0	1.7	0
Feature height (μm)	346.1 ± 6.0	255.7 ± 5.2	249.4 ± 11.8	214.2 ± 4.6	86.9 ± 2.4	190.5 ± 4.7	142.4 ± 3.1

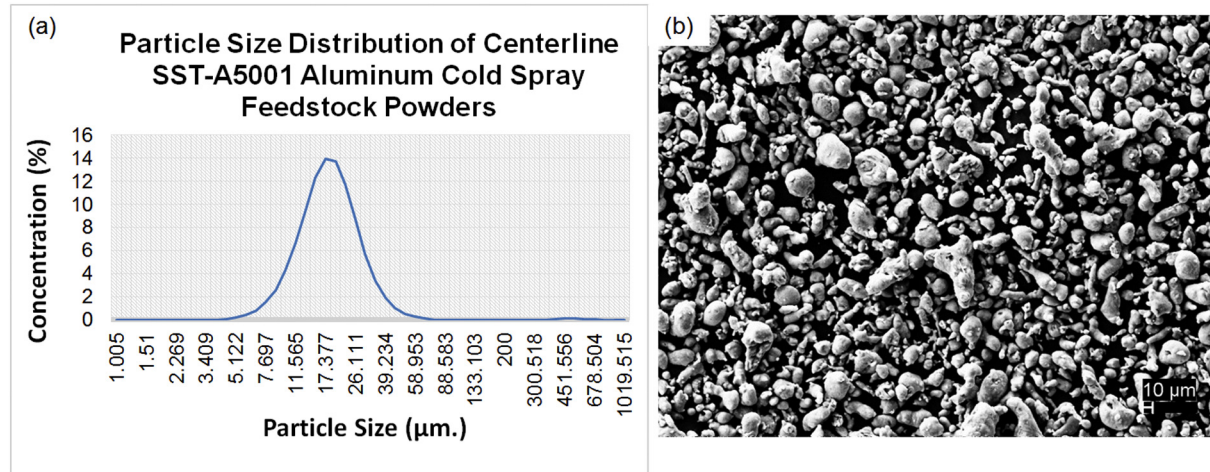


Fig. 1. (a) particle size distribution and (b) SEM image of Centerline SST-A5001 aluminum feedstock powders.

[35]. The statistical analysis was carried out in JMP Pro12. The Monte Carlo simulation and the simulation of particle velocity were both conducted in Matlab.

3. Results and discussion

3.1. Powder morphology and size

The feedstock powders considered for this research were 3 μm, 5 μm, and –45 to +5 μm. Upon simple visual observation, the first two were found to be agglomerated with an appearance of being humid, even after being ultrasonically sieved. Initial coating deposition trials were performed using these powders, which resulted in clogging the system's powder feeder. On the other hand, –45 to +5 μm powders look loose and could be sprayed on the substrates without any problem. The particle size of the –45 to +5 μm powders was examined in the laser scattering particle size analyzer, and the particle size distribution was plotted in Fig. 1(a). The average particle size is 20.4 μm, and the standard deviation is 32.6 μm. The 10th percentile is 10.1 μm, and the 90th percentile is 28.3 μm; which shows that 80% of the actual particles are within 10.1 μm and 28.3 μm range. The measured data correlate with the specification of the –45 to +5 μm powder provided by the vendor. The SEM and ImageJ software were used to analyze the particles' morphology of the SST-A5001 powder. The mean Feret diameter of the particles is 12.8 μm, and the 90% confidence interval is between 11.0 μm and 14.7 μm. These values are within the range of the specification. The difference shown between the results of the laser scattering analyzer and the SEM might be due to the geometries of the particles. The mean roundness was found to be 0.55, and the aspect ratio 2.07 in the SEM analysis, which indicates that these particles are elongated with an irregular morphology as shown in Fig. 1 (b). One benefit of having these irregular morphologies is that it has been reported that powders with irregular morphologies present a higher in-

flight velocity than same-size powders with spherical morphologies [36].

3.2. Screens and substrates

To produce two-dimensional surface features, five meshes, 16, 45, 170, 200, 400, and 5/16" were used as screens to block the sprayed particles from deposition on aluminum, glass, silicon wafer, and printed circuit board (PCB) substrates. A 3D printed 8 mm ABS plastic mesh was considered as a screen to examine the feasibility of using plastic screen for cold spray surface patterning; however, the plastic mesh deformed transiently with impacting particles with gas temperature of 300 °C (Fig. 9), which results in no features patterned on a substrate. To prevent deformation of the plastic mesh, the gas temperature can certainly be reduced below 300 °C, but this will result in no adhesion of aluminum particles to the substrates; therefore, using plastic screen for cold spray surface patterning is determined to be not feasible in our investigation.

Both copper and stainless steel meshes worked very well for spraying aluminum feedstock powders with gas temperatures above 300 °C. All the copper and stainless steel meshes were found to be reusable for multiple experiments; this reusable nature is cost-friendly for the application of cold spray surface patterning. Due to its porosity, the adhesion of a cold sprayed coating to the mesh is poor; even if a coating were formed on top of a fine mesh, it could be removed easily.

Although only metal meshes with square pores and circular pores (one sample was fabricated with a mesh with circular pores) were tested in the present study, the findings can certainly be applicable to metal screens with pores in various morphologies. Metal additive manufacturing techniques can potentially be used to fabricate screens with morphologies of interest.

Results show that two-dimensional features with various geometries could be fabricated on different substrates including aluminum, silicon,



Fig. 2. Two-dimensional features fabricated on aluminum, silicon wafer, glass, and copper foil layer of PCB with cold spray surface patterning technique.

soda-lime glass, and copper foil layer of PCB as shown in Fig. 2. Initially, the nonconductive layer of PCB had been sprayed with aluminum feedstock powders; however, besides the formation of a groove on the substrate caused by erosion from impacting particles, no adhesion of aluminum feedstock powders was obtained. As a result, the copper foil layer was used as a substrate. The sample identification (ID), cold spray processing parameters, and the corresponding feature heights are listed in Table 1 for the aluminum substrate, Table 2 for glass and silicon wafer substrates, and Table 3 for PCB substrate. Detailed discussion on how cold spray processing parameters influence the fabricated two-dimensional features is described in the following sections.

3.3. Pore size and feature size

Part of the objective of this research is to examine how small the two-dimensional features can be fabricated with the cold spray surface patterning technique. Mesh (16, 170, 200, and 400) were used as screens to block the impacting particles from deposition to fabricate two-dimensional surface features on aluminum substrates. During the cold spray surface patterning process, the screens were secured above the substrates with a standoff distance of 2 mm for features fabricated with mesh 16 (samples Al-1, Al-2, and Al-3), and a standoff distance of 0 mm for features fabricated with mesh 170, mesh 200, and mesh 400 (samples Al-4, Al-5, Al-6, Al-7, and Al-8). The pore and wire sizes of the meshes, feature sizes, and feature heights were measured in the SEM and optical profilometer. The sample IDs and the representative average data (with margin of errors) are listed in Table 4, and the corresponding cold spray processing parameters are listed in Table 1. Surface features were created with mesh 16, mesh 170, and mesh 200 successfully, but not with the mesh 400 which has pore size of $37.3 \pm 1.5 \mu\text{m}$ and wire size of $25.5 \pm 0.2 \mu\text{m}$. This result is understandable because reduction of pore size also reduces the probability of

Table 4

Sample IDs, pore size and wire size of meshes (60, 170, and 400), feature size and feature height of the patterns fabricated on aluminum substrate.

Sample ID	Al-1	Al-5	Al-7
Mesh	16	170	200
Pore size (μm)	1087.4 ± 9.7	87.6 ± 0.9	68.0 ± 5.4
Wire size (μm)	588.9 ± 3.6	55.5 ± 0.7	44.8 ± 0.5
Feature size (μm)	1282.5 ± 27.7	100.4 ± 4.3	67.4 ± 3.1
Feature height (μm)	392.3 ± 9.5	12.0 ± 0.8	11.5 ± 2.2

impacting particles passing through the mesh. Once the pore size of a mesh is reduced to a critical size or below, the impacting particles can no longer pass the mesh.

Fig. 3(a), (b), and (c) show the SEM images of mesh 16, mesh 170, and mesh 200 respectively. As shown in the images, the metal wires in mesh 16 and mesh 170 are well-aligned to each other; however, those in mesh 200 appear wavy. These observations are in accordance with expectations based on pore size. The margin of error of pore size in mesh 200 is relatively high compared to the average pore size. This high margin of error was found to influence the margin of error of the feature size accordingly. The features fabricated with mesh 16, mesh 170, and mesh 200, are shown in Fig. 3(d), (e), and (f). Well-defined two-dimensional arrays of features were fabricated, especially the features fabricated with mesh 16, which have distinct square features replicating the square pores of the mesh. Although both features fabricated with mesh 170 and mesh 200 are in well-aligned arrays, each individual feature has irregular morphology. Due to feedstock powder size being relatively big (compared to the pore sizes of mesh 170 and mesh 200), and only a small amount of the impacting particles can be deposited on the substrate to form surface features. Thus, each individual feature was only composed of small amount of particles, resulting in irregular morphology. One interesting observation found in

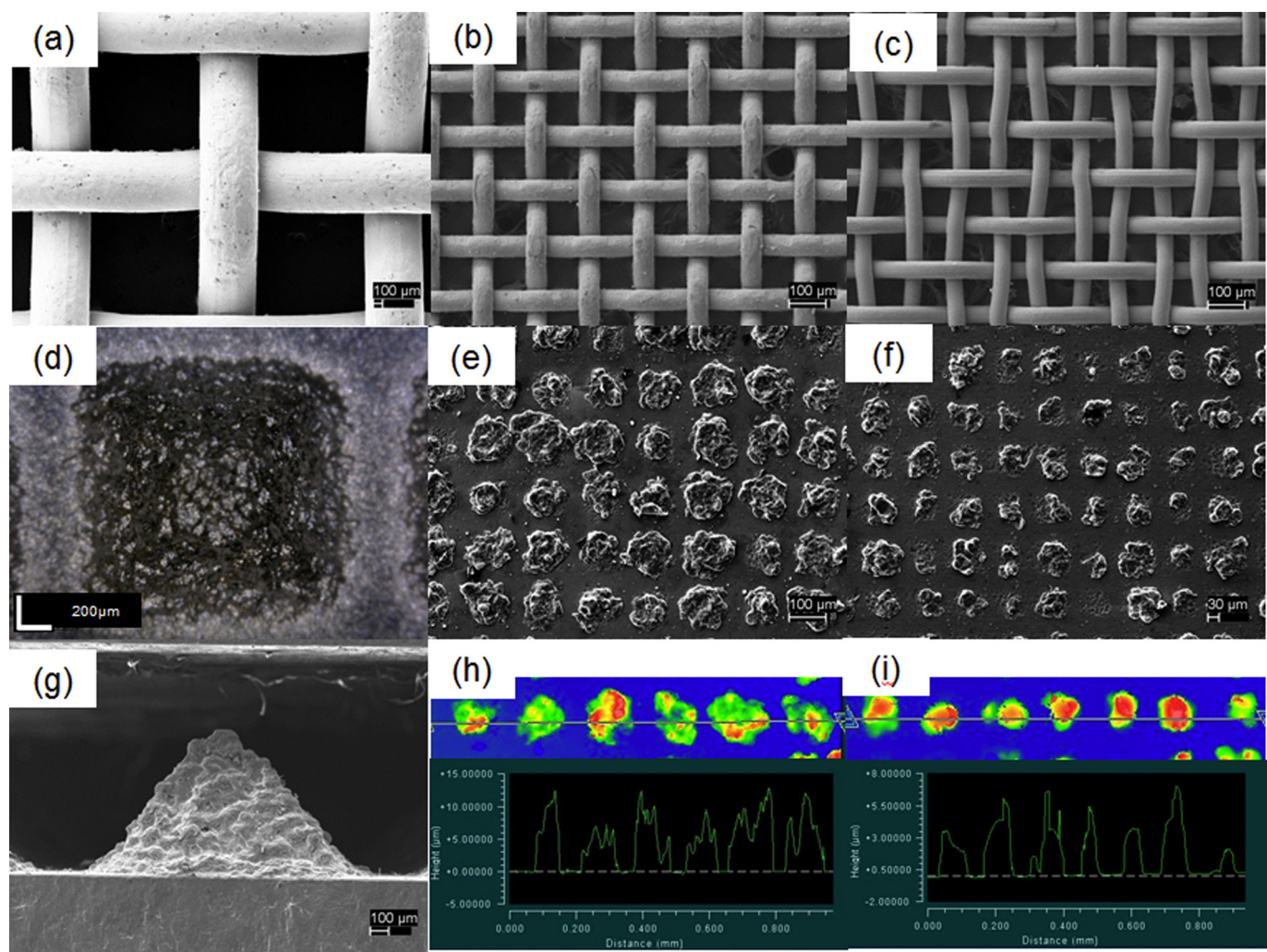


Fig. 3. SEM images show the morphology of (a) mesh 16, (b) mesh 170, and (c) mesh 200; the morphology of the features fabricated with (d) mesh 16, (e) mesh 170, and (f) mesh 200; the topography of the feature fabricated with (g) mesh 16. Line profiles of the feature heights of features fabricated with mesh 170 and mesh 200 obtained by optical profilometer are shown in (h) and (i) respectively.

the features fabricated with mesh 16 and mesh 170 is that the feature size is actually larger than the pore size. The basis of this for mesh 16 is that a 2 mm standoff distance between the mesh and substrate was used during the fabrication process. This small spacing allows small amounts of the impacting particles to get beneath the mesh, leading to larger feature size. However, no standoff distance between the mesh and substrate was used for fabrication of features with mesh 170, so the enlargement of the features is not due to the standoff distance, but possibly the screen (metal mesh) being unsecured during the cold spray surface patterning process. Without proper screen clamping, the patterns cannot be fabricated successfully. Minor movement of a screen might occur during the traverse movement of the gun and result in particles being sprayed underneath the meshes and, therefore enlargement of the feature size. Although both features fabricated with mesh 16 and mesh 170 (samples Al-1 and Al-5) are larger than the pore size, the features fabricated with mesh 200 (sample Al-7) were found to be consistent with average pore size.

As shown in Fig. 4, all feature sizes of sample Al-7 are within the expected range; the mean and variance of the feature and pore size are also very similar. A Two-sample *t*-test was conducted for feature sizes fabricated with mesh 200 and pore size of mesh 200 (sample Al-7). The *p*-value of the *t*-test is 0.84, which is higher than the significance level of 0.05, indicating that the patterned features fabricated with mesh 200 and zero standoff distance replicated the morphology of the pore

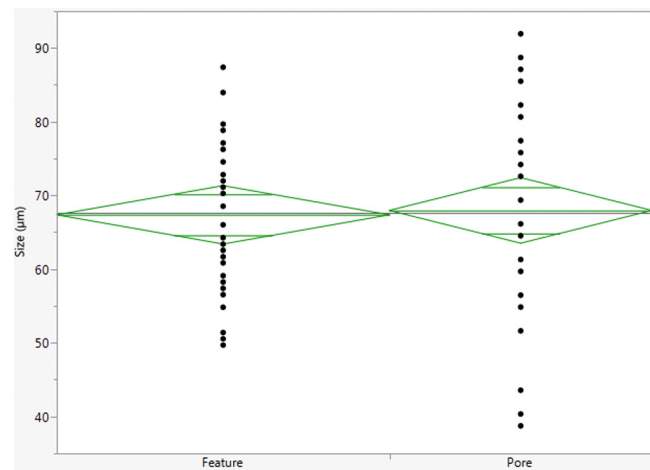


Fig. 4. Distribution of feature size of features fabricated with mesh 200 and pore size of mesh 200. The diamond means show the 95% confidence intervals of individual data set and one way analysis of variance data.

regions of the mesh 200 very well. The smallest features created in the study were fabricated with mesh 200 and have an average feature size of 67.4 μm, which is approximately 3.3 times of the average particle

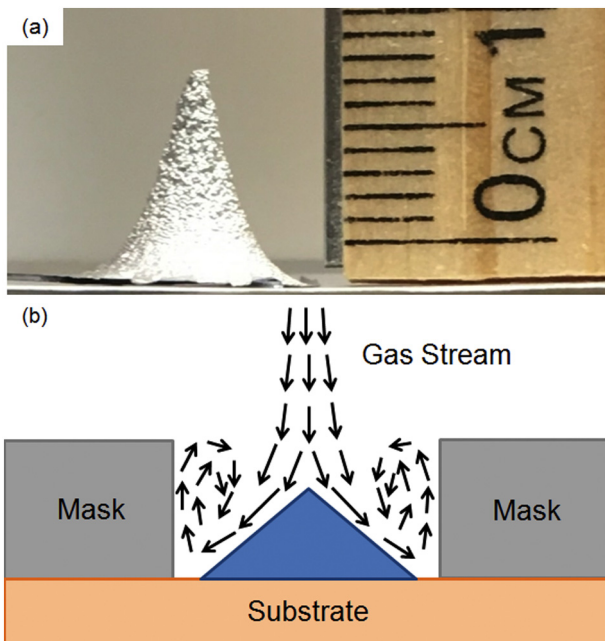


Fig. 5. (a) Optical image of cold sprayed coating at single location with duration of 200 s. (b) Schematic drawing of the recirculation zone near the edges of a screen (not to scale).

size measured from laser scattering analysis. The mesh 400, which was unable to fabricate features, has an average pore size approximately 1.8 times of the average particle size. Based on the above results, in the present study the pore size needs to be larger than 3.3 times the average particle size of feed stock powders in order to have successful deposition of patterned features.

The feature heights of the samples were also examined in the SEM and optical profilometer; the data are shown in Fig. 3(g), (h), and (i). As shown in Fig. 3(g), when the pore size is much bigger than the particle size, the two-dimensional feature tends to form in a pyramid. This observation was also found in the fin arrays produced by Y. Cormier et al. [31–33]. The formation of this pyramid-shaped morphology was not done intentionally. The underlying formation mechanism of this pyramid-shaped morphology is not clear. One observation is worth noting that with a nozzle sitting in one location of a substrate for 200 s, a cone-shaped feature formed; no further adhesion of the impacting particles was observed with increased spraying time (Fig. 5(a)). The angle between the edge of the cone and the horizontal substrate was measured to be approximately 77°. The formation of this inclined edge might be correlated with divergent spray of incident particles. A divergence angle of 6.94° was measured from the cross-section of the nozzle used in the experiment and listed in Table 5. The inclined edge of observed pyramid-shaped morphology might also be correlated with this divergent spray of incident particles. Kim et al. proposed that the recirculation zone shown in Fig. 5(b) played an important role for the formation of the pyramid-shaped morphology [10]. Investigation of

how pyramid-shaped morphology was formed is not within the scope of current work. Detailed investigation of these potential factors needs to be conducted in future study.

The average feature heights fabricated with mesh 170 and mesh 200 were found to be very similar (samples Al-5 and Al-7). The two-sample *t*-test gave a *p*-value of 0.60, which indicates that both feature heights are statistically indistinguishable. The 40 mm/s gun traverse speed, used for the fabrication of features with mesh 200 (sample Al-7) was 2 times higher than the parameter used for the fabrication of features with mesh 170 (sample Al-5). Thus, the duration of the cold spray for mesh 170 should be 2 times higher than the time sprayed with mesh 200. However, this longer duration of the spray was not reflected in the feature heights. One main reason for this is that after one pass of cold spray, both of the tops of the mesh 170 and mesh 200 were fully covered with a layer of cold sprayed coating. This prevented further deposition of any particles; therefore, adjustment of the feature height for mesh smaller than 170 can be challenging. Finer powders with non-agglomerated property might be a potential solution for this problem.

It is worth noting here that changing the screen used for the patterning not only affects the feature size, but also the feature height. Two pairs of samples (Si-4 and Si-6; PCB-1 and PCB-2), which share identical cold spray processing parameters but different mesh size, have different feature heights, as shown in Table 2 and Table 3. The samples (Si-4 and PCB-1) fabricated with mesh 16 have feature heights of $175.2 \pm 5.5 \mu\text{m}$ and $346.1 \pm 6.0 \mu\text{m}$, respectively. In contrast, the samples (Si-6 and PCB-3) fabricated with mesh 45 have feature heights of $156.9 \pm 4.7 \mu\text{m}$ and $249.4 \pm 11.8 \mu\text{m}$. This result shows that the feature height tends to be higher when using bigger meshes (lower mesh numbers). The source of this result is likely due to the formation of a recirculation zone generated near the edges of a mesh. Mesh with smaller pores may lead to a higher backflow of gas stream near a substrate, which reduces the momentum of impacting particles and prevents particles bonding.

The SEM images in Fig. 6(a) and (b) show the aluminum cold sprayed features fabricated with mesh 16 and mesh 45 on a copper foil layer of PCB; Fig. 6(c) and (d) show the aluminum features fabricated with mesh 16 and mesh 45 on a silicon wafer substrate. Both features fabricated with mesh 16 are higher than the ones fabricated with mesh 45. Again, the pyramid-shaped morphologies were found in all the features, despite the substrates used being PCB and silicon wafer rather than aluminum.

3.4. Monte Carlo simulation

In the present study, a Monte Carlo simulation was developed to estimate the probability of feedstock powders passing through the meshes and depositing on the substrates. The simulation uses the particle size distribution measured from laser-scattering analysis, the average wire width, and the average pore size listed in Table 4 as input parameters. The morphologies of particles used in the simulation were all assumed to be spherical. The simulation algorithm was described in following steps. Step 1: A two-dimensional matrix representing a substrate covered with a wire mesh was created with the average wire width and pore size. The value in the matrix is 0 for area without mesh

Table 5

The dimensions of the de Laval nozzle used in the experiments. Note: the dimensions were measure from actual cross-section of the nozzle used. Note: drawing not to scale.

Nozzle parameters	Distance (mm)	
D_i	4.5	
D_t	2.8	
D_e	5.6	
L_a	14.5	
L_b	6.5	
L_c	11.5	
L_d	87.5	

The diagram illustrates the cross-section of a de Laval nozzle. It consists of three main sections: a converging section on the left, a narrowest throat in the middle, and a diverging section on the right. The inner radius of the nozzle is labeled D_i . The distance from the inlet to the throat is L_a . The distance from the throat to the exit is L_b . The outer radius of the nozzle is labeled D_e . The distance from the inlet to the exit is L_d . The distance from the throat to the exit is L_c . The diagram shows the nozzle's profile with hatching indicating the wire mesh structure.

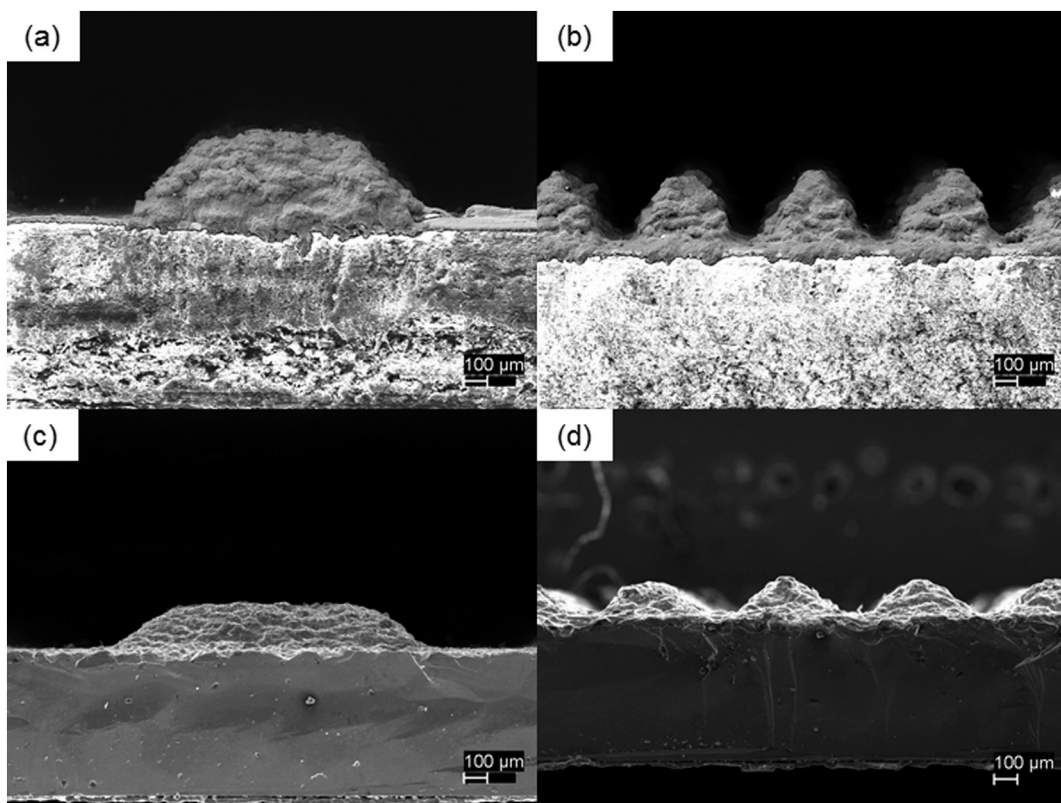


Fig. 6. SEM images of aluminum cold sprayed features fabricated with (a) mesh 16 and (b) mesh 45 on copper foil layer of PCB, and (c) mesh 16 and (d) mesh 45 on silicon wafer substrate.

and 1 for area covered with mesh. Step 2: A random index within the matrix representing the location where the impact of a particle takes place was generated. Step 3: A random number was generated between 1 and 100. This number was used as the percentile to assign the size of simulated particle from the particle size distribution measured from laser-scattering analysis. Step 4: A spherical particle with the assigned particle size generated from the percentile in Step 3 was dropped at the location generated in Step 2. If the particle with assigned size did not overlay with the area covered with the mesh (area with value of 1), the particle passed the mesh. Step 5: The volume of the particle passing the mesh was projected on the underlying two-dimensional matrix to form coating topography. Step 1 through 5 is one Monte Carlo step. In each simulation, 1000 Monte Carlo steps were simulated for mesh 16, mesh 170, mesh 200, and mesh 400; ten simulations were run for each sample. The average probabilities of particles passing the mesh 16, mesh 170, mesh 200, and mesh 400, are 40.4%, 21.9%, 18.2%, and 8.3% respectively. The above probabilities were calculated based on assuming that all passing particles were considered as deposited without taking into account their sizes. T. Schmidt et al. stated an equation to estimate a “critical particle diameter” (d_{crit}) for cold spray deposition [1]. Particles with diameters above the critical particle diameter have slow thermal diffusion which allows localized shear instability to occur at the surface of impacting spherical particles. The equation is listed as follow [1]:

$$d_{crit} = 36 \times \frac{k}{c_p \rho v_{particle}}$$

k is the thermal conductivity, c_p is the specific heat, ρ is the density, and $v_{particle}$ is the particle velocity. To be able to take this critical particle diameter into account in the simulation, the particle velocity needs to be estimated. J. F. Schiel has created a one-dimensional model of the fluid dynamics and particle transport properties to estimate particle velocity of cold sprayed particles for the Centerline SST model series C

Ultilife nozzle [37]. The simulated particle velocities have been compared and show good consistency with the data measured with a laser velocimetry. This model was utilized to estimate the particle velocity with our cold spray processing parameters: aluminum feedstock powders, 200 psi, 300 °C, and transport gas of nitrogen. The particle velocity was estimated to be 558 m/s from the model for all the particles. With the inputs of particle velocity, thermal conductivity, specific heat and density of aluminum in the equation above, the critical particle diameter was estimated to be 5.1 μm, which is below 0.26 percentile of the total particle size distribution measured from laser scattering analysis. Thus, no obvious change was found in the result of Monte Carlo simulation incorporating the critical particle diameter of 5.1 μm. However, if the deceleration of the smaller particles (due to bow-shock near the substrate) is also taken into account; the optimum size range for most materials falls within –45 to 10 μm [1, 38]. If the deposition of the particles in the Monte Carlo simulation is further limited to particle size larger than 10 μm, the deposition probabilities further decrease to 37.8%, 20.6%, 16.3%, and 6.7% for mesh 16, mesh 170, mesh 200, and mesh 400, respectively.

In the simulation, the probability for particles to deposit with mesh 400 is 6.7%, but in actual experimental data there were no features found in samples fabricated with mesh 400. It is possible that the simulation did not take the incident angle of the impacting particles into account. Intuitively if the nozzle was tilted from the normal of the substrate, the pores of the mesh look smaller from line of sight of the nozzle. With part of the impacting particles being tilted relative to the normal of a substrate (not all the particles exiting the nozzle are parallel to the nozzle), the probability of passing through the pores of the mesh can be even lower. Furthermore, the decelerating of sprayed particles due to bow-shock, which can reduce the velocity of smaller impacting particles below critical velocity and result in no adhesion between particles and a substrate, was not considered in the simulation. Some dented marks generated by the impacting particles were observed on

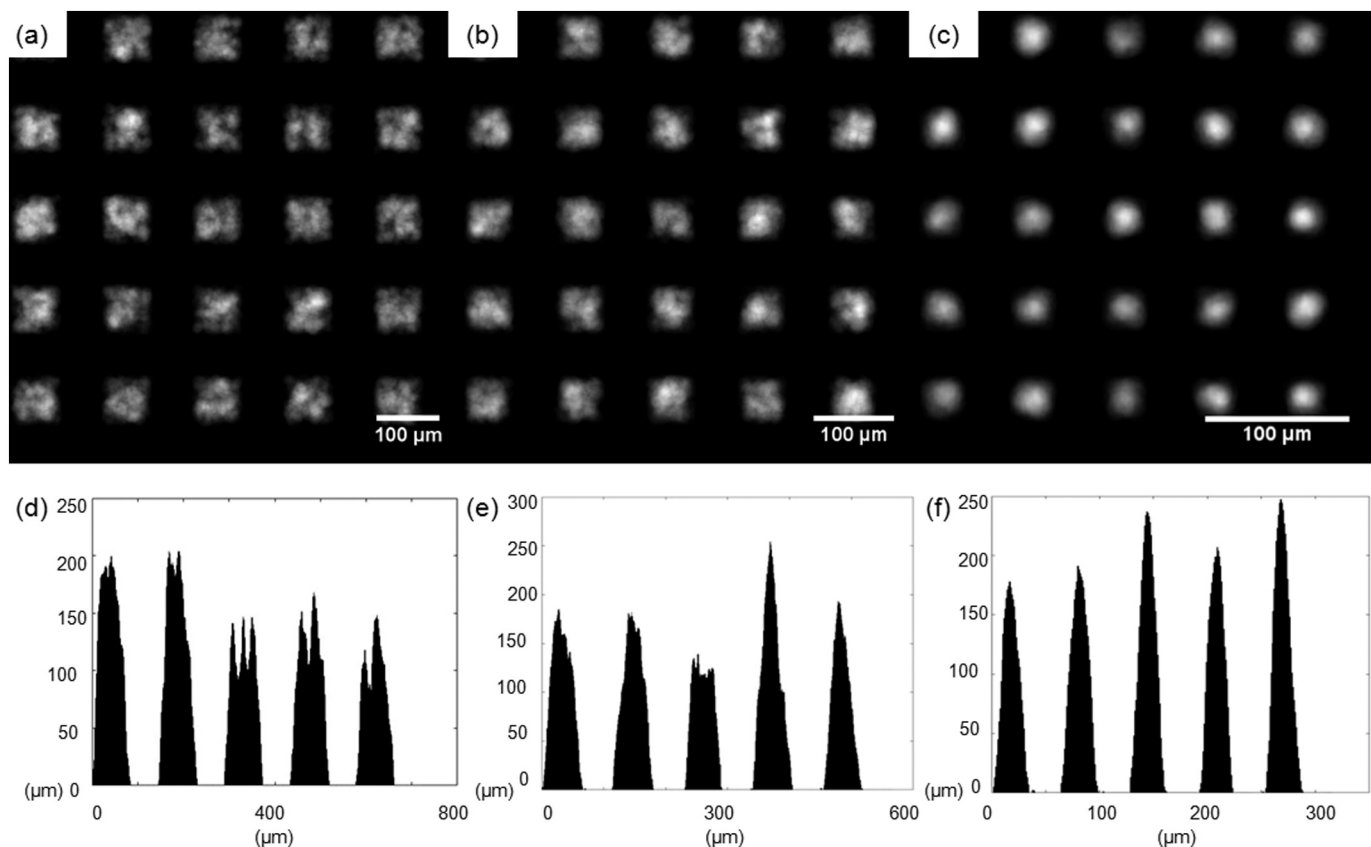


Fig. 7. Simulated features of (a) mesh 170, (b) mesh 200, and (c) mesh 400 by Monte Carlo simulation with 25,000 particles and experimental particle size distribution measured by laser scattering analysis. Successful bonding of particles to the substrates was limited to feedstock powders with particle size of 10 μm and above. The corresponding line profiles of the vertical center features in (a), (b), and (c) are shown in (d), (e), and (f).

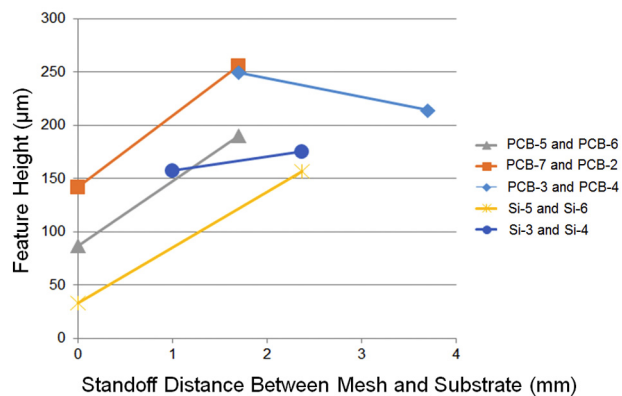


Fig. 8. The feature height versus the standoff distance between mesh and substrate of the five paired data sets fabricated with standoff distance of 0 mm, 1 mm, 1.7 mm, 2.37 mm, and 3.7 mm on PCB and silicon substrates. Each data set comprises a pair of features fabricated with same cold spray processing parameters other than the standoff distance.

the surface of substrate sprayed with mesh 400, but no adhesion of particles was found. This indicates that the particles did get through the mesh 400 but no adhesion was formed. Although, the actual geometry of the feedstock powders was not considered in the simulation, many feedstock powders have elongated irregular shapes (As shown in Fig. 1(b)), which might further prevent the particles passing through the pores. Thus, in reality, the actual deposition probability could be lower than the simulated value of 6.7%.

In addition to the probability of particles passing a mesh, the topography of the features can be simulated in the Monte Carlo

simulation. Since the number of particles leaving the nozzle in an experiment is unknown, the number of Monte Carlo steps for the simulation is also unknown. Therefore, instead of estimating coating thickness of the features only the topography (surface morphology) is meaningful in the simulation. An arbitrary number of Monte Carlo steps, 25,000, was used to simulate the topography of features fabricated with mesh 170, mesh 200, and mesh 400. The corresponding simulated cold sprayed features fabricated with mesh 170, mesh 200, and mesh 400, are shown in Fig. 7(a), (b), and (c). The topography shown in Fig. 7(a) and (b) were found to be similar to the experimental data shown in Fig. 3(e), (f), (h), and (i). The line profiles of the vertical center of the simulated features in Fig. 7(a), (b), and (c) are shown in Fig. 7(d), (e), and (f). The line profiles of the simulated features fabricated with mesh 170 and mesh 200, which are shown in Fig. 7(d) and (e), were also found to be similar to the line profiles of experimental features obtained by an optical profilometer in Fig. 3(h) and (i). These results indicate that the Monte Carlo simulation is effective in estimating the topography of the final features. It is worth noting that the coating thickness of the simulated features and the experimental features was found to be higher at the center of the features and the reason is given as follows. The probability of a bigger particle passing near the center of a pore is higher than the probability of a bigger particle passing near the edge of a pore because the bigger particle may be blocked by the mesh when it travels near the edge of the pore. For example, for a 20 μm particle to pass a 20 μm pore successfully, it has to pass through the center of the pore. If the volume of the particle is projected to a 2-dimensional substrate, consequently a feature with convex shape form at the center of the pore.

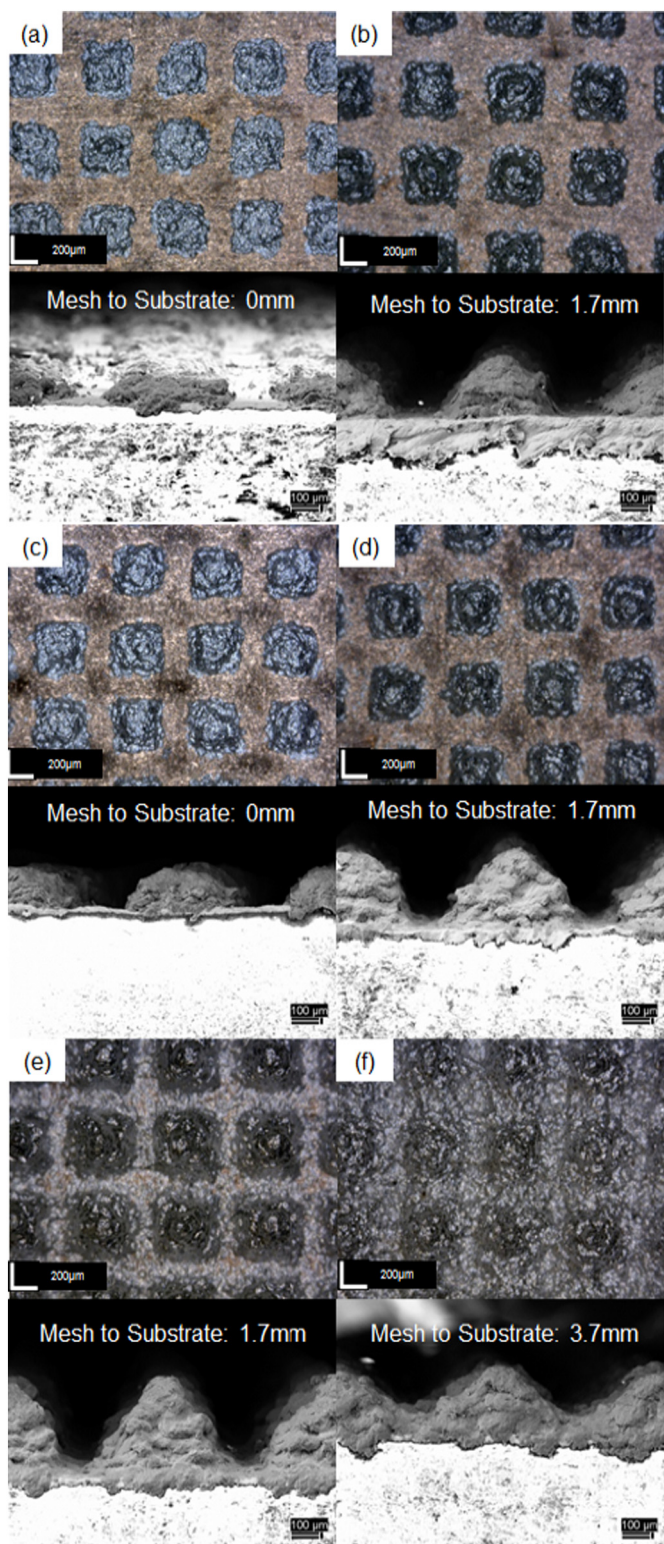


Fig. 9. The samples PCB-5 and PCB-6 fabricated with 0 mm and 1.7 mm standoff distances are shown in (a) and (b); the samples PCB-7 and PCB-2 fabricated with 0 mm and 1.7 mm standoff distances are shown in (c) and (d); the samples PCB-3 and PCB-4 fabricated with 1.7 mm and 3.7 mm standoff distances are shown in (e) and (f). Note: the samples listed here represent the data shown in Fig. 8.

3.5. Standoff distance between mesh and substrate

One aspect of the cold spray surface patterning that was important to investigate was the influence on the morphology of fabricated features exerted by the standoff distance between the mesh and the substrate. The standoff distances of 0 mm, 1 mm, 1.7 mm, 2.37 mm, and 3.7 mm were used for fabrication of aluminum features on copper foil layers of PCB substrates and silicon wafer substrates. Five paired data sets were fabricated (samples PCB-5 and PCB-6, samples PCB-7 and PCB-2, samples PCB-3 and PCB-4, samples Si-5 and Si-6, and samples Si-3 and Si-4), and each data set comprised a pair of features fabricated with the same cold spray processing parameters except for the standoff distances. The details of the cold spray processing parameters of the data sets are listed in [Tables 2 and 3](#). The feature heights versus the standoff distance between mesh and substrate of the five data sets are plotted in [Fig. 8](#). A general trend appears in the plotting, showing that the feature heights increase along standoff distances of 0 mm to ~2.37 mm; however, the feature heights start decreasing with the increase of standoff distances of ~2.37 mm to 3.7 mm. The data appears to support an optimal standoff distance for cold spray surface patterning for fabricating features with maximum feature height. Besides the change of feature height with the standoff distance, it was found that a higher standoff distance between mesh and substrate leads to more particles sprayed beneath the mesh and a smaller separation between the features.

The optical and SEM images in [Fig. 9](#) show the morphology of the patterned features presented the five data sets mentioned above. The samples fabricated with 0 mm and 1.7 mm standoff distances (PCB-5 and PCB-6) are shown in [Fig. 9 \(a\)](#) and [\(b\)](#); the samples fabricated with 0 mm and 1.7 mm standoff distances (PCB-7 and PCB-2) are shown in [Fig. 9\(c\)](#) and [\(d\)](#); the samples fabricated with 1.7 mm and 3.7 mm standoff distances (PCB-3 and PCB-4) are shown in [Fig. 9\(e\)](#) and [\(f\)](#). Reduction in the separation between features correlated with the increase of the standoff distances as observed in [Fig. 9\(a\)](#) through [\(f\)](#). Additionally, the samples fabricated with 0 mm and 2.37 mm standoff distances (Si-5 and Si-6) are shown in [Fig. 10\(a\)](#) and [\(b\)](#); the samples fabricated with 1 mm and 2.37 mm standoff distances (Si-3 and Si-4) are shown in [Fig. 10\(c\)](#) and [\(d\)](#).

The same trend was observed in the features fabricated on the silicon wafer substrate. Observations indicate that with smaller standoff distances between mesh and substrate, the separation between the features becomes more pronounced. Although both feature height and the separation between features are affected by the standoff distances, the morphologies of the features above are all pyramid-shaped, despite the materials of substrates used in the cold spray.

3.6. Gun traverse speed and number of passes

In normal cold spray coating, if the sprayed particles exceed the critical velocity, the coating thickness can be controlled simply by changing the gun's traverse speed and number of passes. The total mass deposit is a simple calculation: feed rate times the distance of travel divided by the gun's traverse speed. With a slow gun traverse speed, or additional passes, more materials can be deposited on a substrate. To examine whether these parameters also influence the feature height, aluminum powders were sprayed with mesh 16 on aluminum substrates with the same cold spray processing parameters except for the gun traverse speeds (samples Al-1 and Al-3). The same type of experiment was also conducted with mesh 45 on copper foil layers of PCB (samples PCB-3 and PCB-6). The cold spray processing parameters and the feature heights are shown in [Table 3](#). Despite the different substrates and meshes used, a general trend was found: When the gun's traverse speed is increased, the dwell time of the nozzle on top of the screens is reduced. In features fabricated with mesh 16, the average feature height dropped from 392.3 to 59.9 μm with an increase of gun traverse speeds of 10 to 20 mm/s; and this held true with the features fabricated with

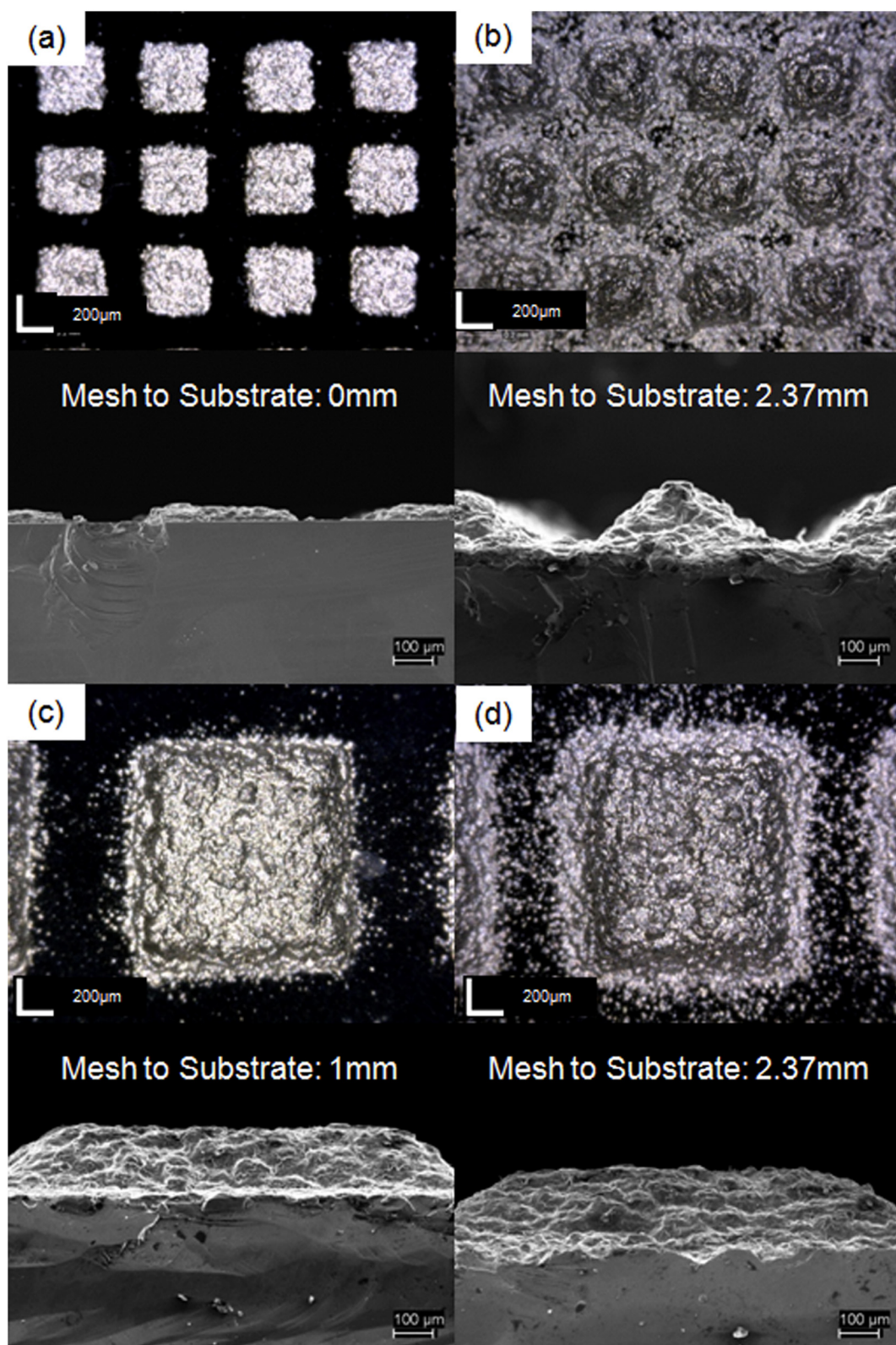


Fig. 10. The samples Si-5 and Si-6 fabricated with 0 mm and 2.37 mm standoff distances are shown in (a) and (b); the samples Si-3 and Si-4 fabricated with 1 mm and 2.37 mm standoff distances are shown in (c) and (d). Note: the samples listed here represent the data shown in Fig. 8.

mesh 45 as well. The average feature height dropped from 249.4 to 190.5 μm with an increase of gun traverse speeds of 20 to 40 mm/s. Thus, the feature height can be reduced by increasing the gun traverse speed.

The morphology of the features was examined in both optical

microscope and SEM. Features fabricated with mesh 16 and gun traverse speeds of 10 and 20 mm/s are shown in Fig. 11(a) and (b). The features fabricated with mesh 45 and gun traverse speeds of 20 and 40 mm/s are shown in Fig. 11(c) and (d). Again, the pyramid-shaped morphologies were found in the features. Modifications in cold-spray

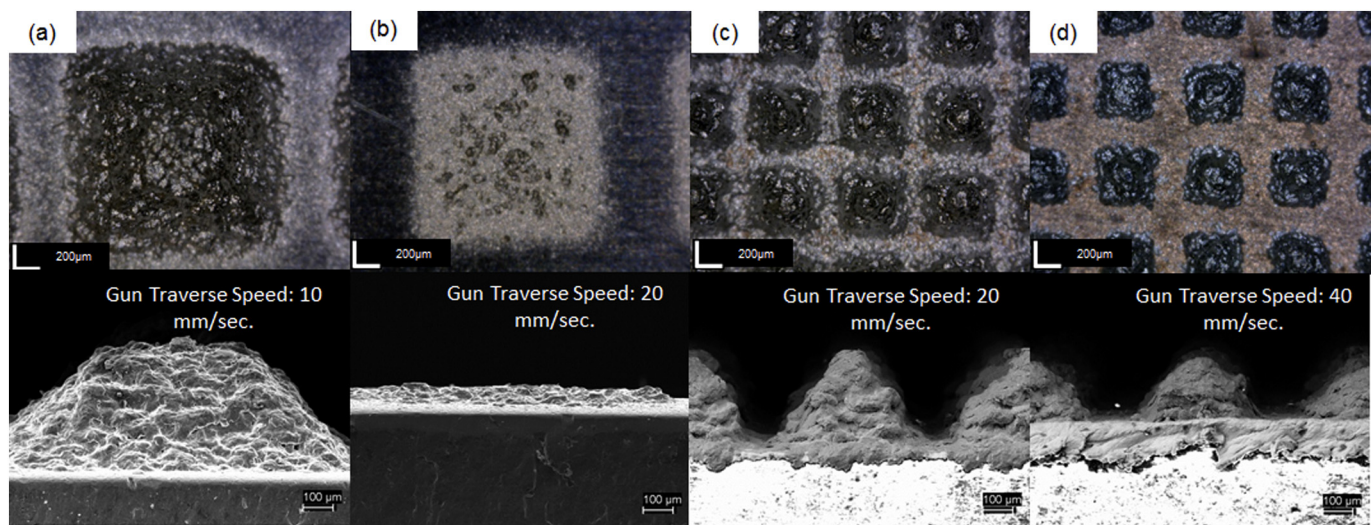


Fig. 11. Optical Images and SEM images of aluminum features fabricated with mesh 16 and gun traverse speed of (a) 10 mm/s. and (b) 20 mm/s; with mesh 45 and gun traverse speed of (c) 20 mm/s. and (d) 40 mm/s.

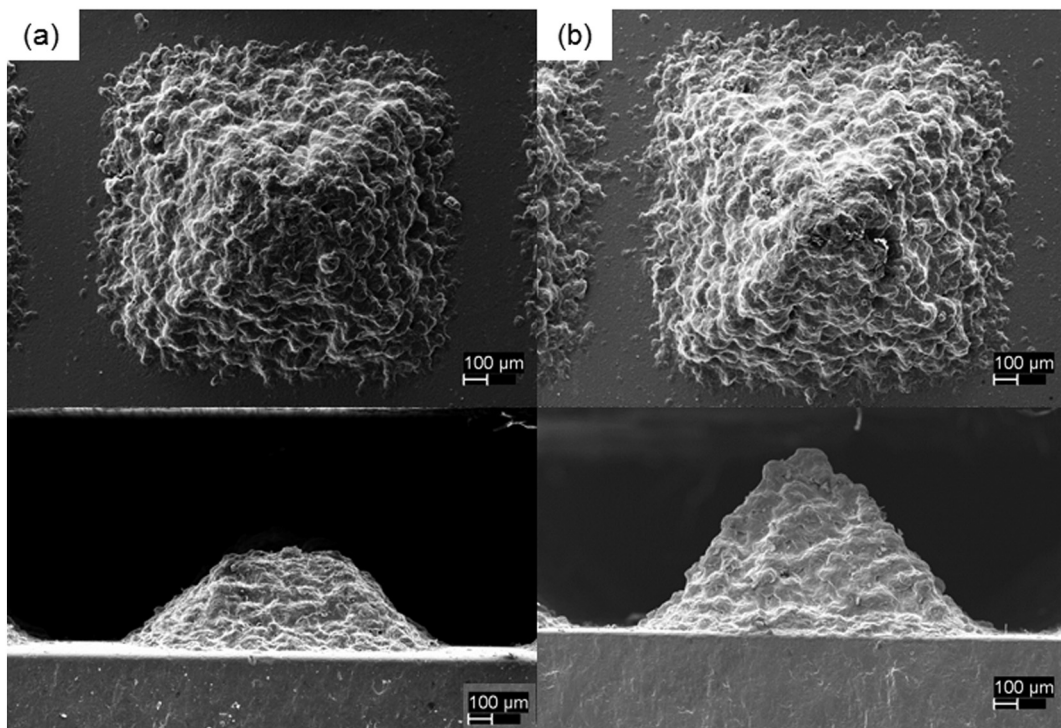


Fig. 12. SEM images of aluminum features fabricated with (a) one pass and (b) two passes.

processing parameters produced no changes in the pyramid-shaped morphology.

The influence of the number of passes was examined by spraying one and two passes of aluminum powders with mesh 16 on aluminum substrates with the same cold-spray processing parameters (samples Al-1 and Al-2) as shown in Table 1.

The feature fabricated with one pass is shown in Fig. 12(a), and the one with two passes is shown in Fig. 12(b). The height of the two dimensional features fabricated with one pass was $392.3 \pm 9.5 \mu\text{m}$; the height of the features fabricated with two passes was $760.6 \pm 9.5 \mu\text{m}$. Although the features fabricated with two passes were higher, the feature height was not proportional to the number of passes. The morphologies of the features were examined with the SEM. The morphologies of both features stayed as pyramids, but the angles

between the edges of the features and the substrates increased from 40° to 52° with spray increase of one pass to two passes. As having the morphology of a pyramid (flat pyramid), the top flat area reduces with the increase of the feature height, which means that less flat area is available for cold-spray deposition. Once a feature reaches a critical height, no further deposition can occur and, the feature will ultimately form a pyramid with sharp tip on top. As shown in Fig. 12(b), there is no flat area remaining on top of the pyramid-shaped feature; because of this geometry, the impacting particle will simply bounce off the feature rather than adhere to it. A similar result was also found in one-dimensional features fabricated by Kim et al. They reported that the aspect ratio (feature height divided by feature width) of the copper electrodes deposited by cold spray increases with number of passes [10]. With seven passes, a film formed at the tip of prism-shaped copper

electrode [10]. The formation of pyramid-shaped geometry in the two-dimensional features limited the addition of feature heights. This explains why the average feature heights fabricated with two passes is not equal to twice the average feature heights fabricated with one pass. This limitation of feature heights, due to the pyramid-shaped morphology, might limit the application of cold-spray surface patterning. Tilting of the nozzle or the substrate might resolve the issue, but further investigation is needed to address this problem.

4. Conclusion

The current study presents the feasibility of fabricating two-dimensional features with aluminum feedstock powders on aluminum, silicon, soda-lime glass, and copper foil layers of PCB substrates. It was found that the two-dimensional features could be fabricated with copper and stainless steel screens on the substrates listed above. More precisely features could be fabricated with mesh 16, mesh 45, mesh 170, and mesh 200, but not mesh 400. The smallest features that could be fabricated with 45 to +5 µm feedstock powders had an average feature size of $67.4 \pm 3.1 \mu\text{m}$. The smallest mesh pore size needs to be approximately 3.3 times larger than the average feedstock powders particle size in order to have successful deposition. The feature height was found to be influenced by the mesh number, the standoff distance between mesh and substrate, the gun's traverse speed, and the number of passes. Generally speaking, smaller mesh numbers, slower gun traverse speeds, and higher numbers of passes result in higher feature heights. There is an optimal standoff distance between mesh and substrate for fabricating features with optimal deposition efficiency. Additionally, the standoff distance between the mesh and substrate influences the feature size and the separation between features. With a high standoff distance, feature size increases and overlapping occurs. To have optimal separation between features and an optimal replication of the morphology of a mesh, zero standoff distance between mesh and substrate should be used. All the features fabricated in the investigation displayed pyramid-shaped morphology. The maximum feature height is limited by the pyramid-shaped morphology. For fabrication with mesh 170 or higher, the feature height was further limited by cold sprayed coating formed on the fine mesh.

The Monte Carlo simulation, incorporating the measured particle size distribution and the geometries of the metal screens, demonstrated to be a useful tool for estimating the probability of feedstock powders passing through the meshes. Despite the coating thickness cannot be estimated due to unknown of total number of particles exiting the nozzle during an experiment, both the morphologies and the line profiles of simulated features fabricated with mesh 170 and mesh 200 showed good correlation with the experimental data, indicating that the Monte Carlo simulation is also a valuable tool for the simulation and visual inspection of surface morphology and topography of features fabricated by the cold-spray surface patterning technique.

Acknowledgement

This work was funded by the Department of Mechanical and Aerospace Engineering of the Naval Postgraduate School. All the samples with surface features were fabricated in the cold spray lab and all the materials characterization was conducted in the Center for Materials Research in the Naval Postgraduate School.

References

- [1] T. Schmidt, F. Gärtner, H. Assadi, H. Kreye, Development of a generalized parameter window for cold spray deposition, *Acta Mater.* 54 (2006) 729–742, <http://dx.doi.org/10.1016/j.actamat.2005.10.005>.
- [2] R.C. Dykhuisen, M.F. Smith, Gas dynamic principles of cold spray, *J. Therm. Spray Technol.* 7 (1998) 205–212, <http://dx.doi.org/10.1361/105996398770350945>.
- [3] F. Gärtner, T. Stoltenhoff, T. Schmidt, H. Kreye, The cold spray process and its potential for industrial applications, *J. Therm. Spray Technol.* 15 (2006) 223–232, <http://dx.doi.org/10.1361/105996306X108110>.
- [4] H. Assadi, F. Gärtner, T. Stoltenhoff, H. Kreye, Bonding mechanism in cold gas spraying, *Acta Mater.* 51 (2003) 4379–4394, [http://dx.doi.org/10.1016/S1359-6454\(03\)00274-X](http://dx.doi.org/10.1016/S1359-6454(03)00274-X).
- [5] T. Stoltenhoff, H. Kreye, H.J. Richter, An analysis of the cold spray process and its coatings, *J. Therm. Spray Technol.* 11 (2002) 542–550, <http://dx.doi.org/10.1361/105996302770348682>.
- [6] M. Grujicic, C.L. Zhao, W.S. DeRosset, D. Helfritch, Adiabatic shear instability based mechanism for particles/substrate bonding in the cold-gas dynamic-spray process, *Mater. Des.* 25 (2004) 681–688, <http://dx.doi.org/10.1016/j.matdes.2004.03.008>.
- [7] M. Grujicic, J.R. Saylor, D.E. Beasley, W.S. DeRosset, D. Helfritch, Computational analysis of the interfacial bonding between feed-powder particles and the substrate in the cold-gas dynamic-spray process, *Appl. Surf. Sci.* 219 (2003) 211–227, [http://dx.doi.org/10.1016/S0169-4332\(03\)00643-3](http://dx.doi.org/10.1016/S0169-4332(03)00643-3).
- [8] A. Moridi, S.M. Hassani-Gangaraj, M. Guagliano, M. Dao, Cold spray coating: review of material systems and future perspectives, *Surf. Eng.* 30 (2014) 369–395, <http://dx.doi.org/10.1179/1743294414Y.00000000270>.
- [9] R.N. Raeolison, C. Verdy, H. Liao, Cold gas dynamic spray additive manufacturing today: deposit possibilities, technological solutions and viable applications, *Mater. Des.* 133 (2017) 266–287, <http://dx.doi.org/10.1016/j.matdes.2017.07.067>.
- [10] D.-Y. Kim, J.-J. Park, J.-G. Lee, D. Kim, S.J. Tark, S. Ahn, J.H. Yun, J. Gwak, K.H. Yoon, S. Chandra, S.S. Yoon, Cold spray deposition of copper electrodes on silicon and glass substrates, *J. Therm. Spray Technol.* 22 (2013) 1092–1102, <http://dx.doi.org/10.1007/s11666-013-9953-4>.
- [11] S.M. Hassani-Gangaraj, A. Moridi, M. Guagliano, Critical review of corrosion protection by cold spray coatings, *Surf. Eng.* 31 (2015) 803–815, <http://dx.doi.org/10.1179/1743294415Y.0000000018>.
- [12] V.K. Champagne, B. Gabriel, J. Villafuerte, 15 - Cold Spray Coatings to improve the corrosion resistance of magnesium (Mg) alloys, (2013), <http://dx.doi.org/10.1533/9780857098962.3.414>.
- [13] K.B. Perez, C.B. Williams, Combining additive manufacturing and direct write for integrated electronics – a review, *Int. Solid Free. Fabr. Symp. Proc.* (2013) 962–979.
- [14] P. Richer, M. Yandouzi, L. Beauvais, B. Jodoin, Oxidation behaviour of CoNiCrAlY bond coats produced by plasma, HVOF and cold gas dynamic spraying, *Surf. Coatings Technol.* 204 (2010) 3962–3974, <http://dx.doi.org/10.1016/j.surcoat.2010.03.043>.
- [15] W.R. Chen, E. Irisson, X. Wu, J.G. Legoux, B.R. Marple, The oxidation behavior of TBC with cold spray CoNiCrAlY bond coat, *J. Therm. Spray Technol.* (2011) 132–138, <http://dx.doi.org/10.1007/s11666-010-9601-1>.
- [16] D.J. Park, H.G. Kim, Y. Il Jung, J.H. Park, J.H. Yang, Y.H. Koo, Behavior of an improved Zr fuel cladding with oxidation resistant coating under loss-of-coolant accident conditions, *J. Nucl. Mater.* 482 (2016) 75–82, <http://dx.doi.org/10.1016/j.jnucmat.2016.10.021>.
- [17] N. Matthews, Cold spray applications for the Australian defence department, *Int. Therm. Spray Conf. Expo.* 2012 (2012).
- [18] A. Sova, S. Grigoriev, A. Okunkova, I. Smurov, Potential of cold gas dynamic spray as additive manufacturing technology, *Int. J. Adv. Manuf. Technol.* 69 (2013) 2269–2278, <http://dx.doi.org/10.1007/s00170-013-5166-8>.
- [19] M.E. Lynch, W. Gu, T. El-Wardany, A. Hsu, D. Viens, A. Nardi, M. Klecka, Design and topology/shape structural optimisation for additively manufactured cold sprayed components, *Virtual Phys. Prototyp.* 8 (2013) 213–231, <http://dx.doi.org/10.1080/17452759.2013.837629>.
- [20] Y. Zabila, M. Perzanowski, A. Dobrowolska, M. Kac, A. Polit, M. Marszałek, Direct laser interference patterning: theory and application, *Acta Phys. Pol. A* (2009) 591–593.
- [21] K. Seshan, *Handbook of Thin Film Deposition*, (2012), <http://dx.doi.org/10.1016/B978-1-4377-7873-1.00006-1>.
- [22] M. Henini, *Handbook of thin-film deposition processes and techniques*, *Microelectron. J.* 31 (2000) 219, [http://dx.doi.org/10.1016/S0026-2692\(99\)00122-6](http://dx.doi.org/10.1016/S0026-2692(99)00122-6).
- [23] D.L. Smith, D.W. Hoffman, Thin-film deposition: principles and practice, *Phys. Today* 49 (1996) 60, <http://dx.doi.org/10.1063/1.2807590>.
- [24] M.M. Ling, Z. Bao, Thin film deposition, patterning, and printing in organic thin film transistors, *Chem. Mater.* 16 (2004) 4824–4840, <http://dx.doi.org/10.1021/cm0496117>.
- [25] L.R. Harriott, Limits of lithography, *Proc. IEEE* 89 (2001) 366–374, <http://dx.doi.org/10.1109/5.915379>.
- [26] M. Köhler, Wet-chemical etching methods, *Etch. Microsyst. Technol.* (1999) 29–110, <http://dx.doi.org/10.1002/9783527613786.ch3>.
- [27] P. Verdonck, Chap 10, Plasma Etching, Of. Microfabricação Proj. E Construção de CI's MOS, 2006, pp. 1–11, , <http://dx.doi.org/10.1016/j.tsf.2005.12.196>.
- [28] D.M. Mattox, *Handbook of Physical Vapor Deposition (PVD) Processing*, (1998), <http://dx.doi.org/10.1016/B978-081551422-9.50014-0>.
- [29] H.O. Pierson, W.A. Publishing, N. York, *Handbook of Chemical Vapor Deposition (CVD)*, (1999), <http://dx.doi.org/10.1016/B978-081551432-9.50004-8>.
- [30] S.V. Klinkov, V.F. Kosarev, N.S. Ryashin, V.S. Shikalov, Experimental study of cold gas spraying through a mask. Part 1, Thermophys. Aeromech. 23 (2016) 735–740, <http://dx.doi.org/10.1134/S0869864316050115>.
- [31] Y. Cormier, P. Dupuis, B. Jodoin, A. Corbeil, Net shape fins for compact heat exchanger produced by cold spray, *J. Therm. Spray Technol.* 22 (2013) 1210–1221, <http://dx.doi.org/10.1007/s11666-013-9968-x>.
- [32] Y. Cormier, P. Dupuis, B. Jodoin, A. Corbeil, Mechanical properties of cold gas dynamic-sprayed near-net-shaped fin arrays, *J. Therm. Spray Technol.* 24 (2014) 476–488, <http://dx.doi.org/10.1007/s11666-014-0203-1>.
- [33] Y. Cormier, P. Dupuis, A. Farjam, A. Corbeil, B. Jodoin, Additive manufacturing of pyramidal pin fins: height and fin density effects under forced convection, *Int. J. Heat Mass Transf.* 75 (2014) 235–244, <http://dx.doi.org/10.1016/j.ijheatmasstransfer.2014.03.053>.
- [34] O.F.K. and T.V.B. A. I. Kashirin, Apparatus for gas-dynamic coating, US Patent 6402050, 2002.

- [35] C.A. Schneider, W.S. Rasband, K.W. Eliceiri, NIH image to ImageJ: 25 years of image analysis, *Nat. Methods* 9 (2012) 671–675, <http://dx.doi.org/10.1038/nmeth.2089>.
- [36] X.J. Ning, J.H. Jang, H.J. Kim, The effects of powder properties on in-flight particle velocity and deposition process during low pressure cold spray process, *Appl. Surf. Sci.* 253 (2007) 7449–7455, <http://dx.doi.org/10.1016/j.apsusc.2007.03.031>.
- [37] J.F. Schiel, The cold gas-dynamic spray and characterization of microcrystalline austenitic stainless steel, Naval Postgraduate School, 2014 <http://hdl.handle.net/10945/43994>.
- [38] J. Pattison, S. Celotto, A. Khan, W. O'Neill, Standoff distance and bow shock phenomena in the Cold Spray process, *Surf. Coatings Technol.* 202 (2008) 1443–1454, <http://dx.doi.org/10.1016/j.surcoat.2007.06.065>.